

Optomechanical Alignment Instability in LIGO Mode Cleaners

Jenne Driggers

LIGO REU / SURF Summer 2006

Mentor: Alan Weinstein

Co-Mentor: Rana Adhikari

21 September 2006

Abstract

In order to increase sensitivity to weak gravitational wave signals in the Laser Interferometer Gravitational Wave Observatory (LIGO) it is important to reduce all noise sources. In particular, core optics hang from pendulums to mechanically filter seismic noise. In combination with the high-powered laser used in the interferometer, these pendulum systems can cause an interesting problem. If the laser beam is not hitting the mirror in the center, the radiation pressure of the light can push the mirror out of alignment. If the torque due to the laser light is larger than the restoring and damping torques of the pendulum and the servo, the cavity can become unstable. As LIGO prepares to upgrade its system, including adding higher-powered lasers, it is useful to determine if the higher power will cause the cavities to become unstable. We are developing a model of this optomechanical alignment system to study the instability and determine the specifications of a servo to control it. We have also assembled and used a laser-based system to test the photodiodes in the servos that control the interferometer, including the mode cleaner servo, and have built and implemented a low-pass filter to improve the gain of the mode cleaner servo as part of an effort to measure and model this instability.

Background and Motivation:

Gravitational waves have been predicted since Einstein's Theory of General Relativity¹, although they have yet to be directly observed. The Laser Interferometer Gravitational Wave Observatory (LIGO) has been designed to, and is working toward, observing gravitational waves (GW) from astrophysical sources such as black hole / black hole mergers and neutron star / neutron star mergers, and others². LIGO utilizes a Fabry-Perot Michelson Interferometer for its measurements which, among other things, implies that the mirrors suspended in the interferometer must be carefully controlled such that the laser light resonates as desired in each optical cavity³. To decrease noise in measurements, LIGO utilizes a three mirror ring cavity as a mode cleaner to filter out all but the TEM₀₀ transverse mode of the light, and to stabilize the frequency of the laser. When the LIGO interferometers are in science mode and a GW encounters an interferometer, the GW will produce differential changes in the lengths of the two arms. The length of one arm will be slightly increased, while the length of the other arm will be slightly decreased⁴. This will alter the interference that results from recombining the light from the different cavities, and some light will emerge from the darkport where previously there was complete destructive interference. We can then measure the interference at the darkport, which will tell us about the GWs³.

The entire LIGO project is a very large-scale endeavor. In Livingston, Louisiana and Hanford, Washington there are LIGO interferometers with 4km arms (Hanford also has a 2km interferometer). While these sites are currently operating, work is being done to upgrade these interferometers to increase their sensitivity to gravitational waves. Within a few years Initial LIGO (the current configuration) will upgrade to “Enhanced LIGO”, and the interferometers will incorporate some of the features of the final upgrade plan. The fully upgraded interferometers will be titled “Advanced LIGO”, or AdLIGO, and should be commissioned a few years after Enhanced LIGO. Caltech is home to a smaller prototype version of the full interferometers, having arms of 40m. The Caltech 40m interferometer is a research and development testbed for improvements that will be incorporated into the AdLIGO interferometers. The goal of all of the ongoing work in the 40m lab is to understand how to control and optimize the 40m interferometer at Caltech, so that when the LIGO sites are upgraded to become Advanced LIGO, we will already have an idea of how to use and control them.

The lasers used for the interferometers will be one of the components that will be upgraded for both Enhanced and Advanced LIGO. For Initial LIGO, the lasers are 10W Nd:YAG lasers, with a wavelength of 1064nm. For Enhanced and Advanced LIGOs, the wavelength will stay constant, but the power will increase to 30W for Enhanced LIGO, and 200W for Advanced LIGO. A significant controls question is whether or not the new higher powered lasers will produce enough torque to cause the suspended mirrors to fall out of alignment. While this phenomenon has been fairly thoroughly examined for the arms of all the upgrades of LIGO, the instability in the mode cleaners is still an open question. Questions include whether the mode cleaners, according to their current specifications, are expected to be unstable, and what can be done to successfully control the instability without hurting the noise limits and sensitivities of the interferometers.

Radiation Pressure and Instabilities

The core optics in all of the LIGO interferometers are suspended as pendulums within the vacuum chambers, and have servos to control their longitudinal position, as well as their pitch and yaw angles. Angular displacement from the desired orientation is corrected by the application of torque. There are three torques acting on each optic: two of which are restoring, and one of which is sometimes restoring and sometimes not restoring. The torques due to the pendulum and the controls servo are restoring torques, while the torque due to radiation pressure is either restoring or not, depending on the mode. The torque due to radiation pressure is given by $\tau_{radiation} = \frac{2Px}{c}$, where P is the

power hitting the mirror, x is the distance from the axis of rotation, and c is the speed of light⁵. For the case of LIGO, with Fabry-Perot cavities and suspended optics, P is the power circulating in the cavity, and x is the beam’s distance from the center of the mirror.

For a two mirror resonant optical cavity like the LIGO interferometer arms, there are two modes each for pitch and yaw that the radiation pressure can excite. One of these modes is self-aligning (Figure 1), and the other is unstable (Figure 2)⁶. The orientation of the optical axis is defined by the mirrors’ centers of curvature. The optical axis in a two mirror cavity is defined by the centers of curvature of the mirrors, so if the mirrors are tilted, thus moving the centers of curvature, the optical axis must change positions, as in Figure 1 and Figure 2.

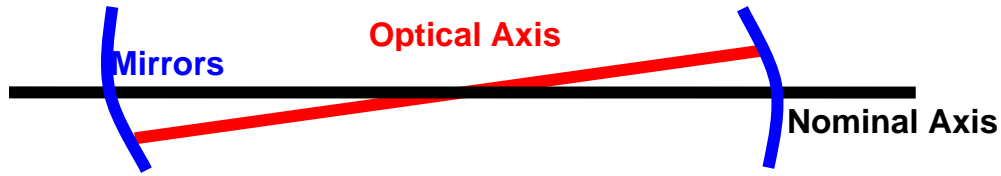


Figure 1: Self-aligning mode excited by radiation pressure. The mirrors tilt in the same way, the optical axis tilts, and the light applies torque to push the mirrors back to their original positions⁶.

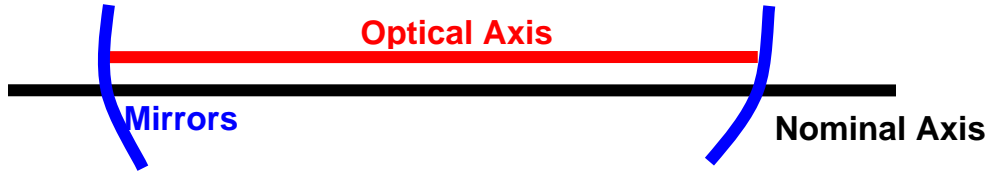


Figure 2: Unstable mode excited by radiation pressure. The mirrors tilt in opposite directions, and the optical axis moves up and puts more torque on the mirrors in the same direction, and pushes them farther out of alignment⁶.

For a three mirror cavity such as the LIGO mode cleaners (Figure 3), there are slightly more complicated analogous modes excited by the radiation pressure for both pitch and yaw. It seems clear from the two mirror case that the beam position on the mirror, which determines the radiation torque on the mirror, is dependent on the positions of all the mirrors in the cavity. For the mode cleaners, there are 2 flat mirrors positioned close together labeled MC1 and MC3, and a curved mirror, MC2. The more involved description of the relative positions of the mirrors in a three mirror cavity translates to a more complex description of the beam position on any given mirror in the cavity, and a more complex description of the torques on the mirrors, which defines the more complicated modes excited by the radiation pressure.

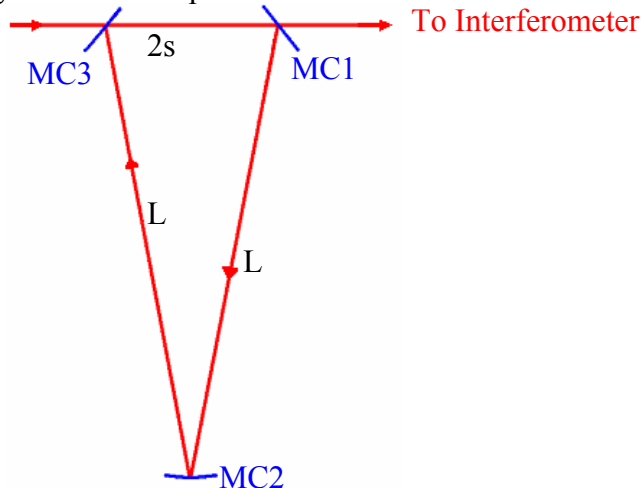


Figure 3: Schematic of LIGO mode cleaner, a three mirror ring cavity. The two top flat mirrors are partially transmitting with $T=0.2\%$ (MC1, MC3), and the bottom mirror is curved (MC2). Light comes in from the left, circulates between MC1, MC2, MC3 and back to MC1 before eventually exiting through MC1 toward the main interferometer.

The natural pendulum torque is given by $\tau_{pendulum} = \alpha I \omega_{pendulum}^2$, where α is the angle of the mirror from the nominal axis, I is the moment of inertia of the mirror and $\omega_{pendulum}$ is the natural pendulum frequency of the suspended optic. This torque is always a restoring torque to move the mirror back to its nominal position, with the center of curvature on the nominal axis. If there were no torques acting on the mirror other than the pendulum torque, the mirror would see a resonant peak at the pendulum frequency. When the radiation torque is added, the resonant peak can change positions. The torque due to the damping servo acts to soften the shape of the peak, i.e. flatten it out so the mirror does not resonate so strongly, but it does not in general change the position of the peak.

Potential Instabilities and Solutions in LIGO Interferometers

Many of the significant cavities in the LIGO interferometers have been studied to check on their potential instabilities. It has been noticed that the Initial LIGO mode cleaners are stable, but the Initial LIGO arms are not stable without damping servos. For a misalignment of the mirrors in the Initial LIGO arms of 1 degree, the torque due to radiation with a full 14kW of power in the 4km arms on either Input Test Mass is 0.0143N*m, while the pendulum torque is 0.0082N*m. The instability in the Initial LIGO arms was first noticed in the Hanford 2km interferometer in 2002⁷. It has been calculated that the Enhanced LIGO and Advanced LIGO interferometer arms will be unstable, but it has not been determined if the mode cleaners for those upgrades will be unstable or not. Calculations have been done, and a model created (discussed later) to help with this determination.

Although we know that if the interferometers did not have damping servos many of the cavities would be unstable, we are confident that it is possible to create servos strong enough to keep those instabilities under control. Unfortunately, strength is not the only feature the controls servos must have. The noise in the Wave Front Sensors (WFS) must be kept low to avoid polluting the laser frequency stabilization servo. Lowering the WFS noise to an acceptable level for Initial LIGO was successfully done using filters to help roll off the noise faster⁷.

Filters are only capable of rolling any signal, including noise, off at a certain rate, which translates to a certain slope on a plot in terms of frequency. This implies that for the case of Advanced LIGO, where we hope to be sensitive to gravitational waves as low as 10Hz, with a much smaller noise strain, there will not be enough 'distance' in terms of frequency to lower the noise from the current WFS servos to an acceptable level. The question of how to create servos with high enough bandwidth to control the cavities while maintaining a very low level of noise is an open one, and further work must be done in this area⁷.

Time-Domain Model of Mode Cleaner Cavities

To help determine if instability due to radiation pressure is a significant concern for the Enhanced and Advanced LIGO mode cleaners, a time-domain model has been created to model the various features of the suspended optics, the controls servos, and the radiation pressure acting on the mirrors. This model (Figure 4) was created using Simulink, the time-domain modeling feature of MATLAB. A major benefit of this model is that it will be possible to build around it, and incorporate more features of the

interferometer, to better model the system as a whole. It will be particularly useful to incorporate a triple-pendulum system into the suspensions of this model, such that the Advanced LIGO case can be modeled more accurately. The model is called by a MATLAB script, which first defines the parameters of the particular cavity to be modeled. The generic properties of any LIGO mode cleaner are incorporated into the Simulink model, but the parameters unique to each cavity, including the length of the cavity, the mirror dimensions and which degree of freedom to be examined, are defined in an external MATLAB script, which makes it more convenient to quickly model the mode cleaner cavities for all of the LIGO upgrades, in either pitch or yaw.

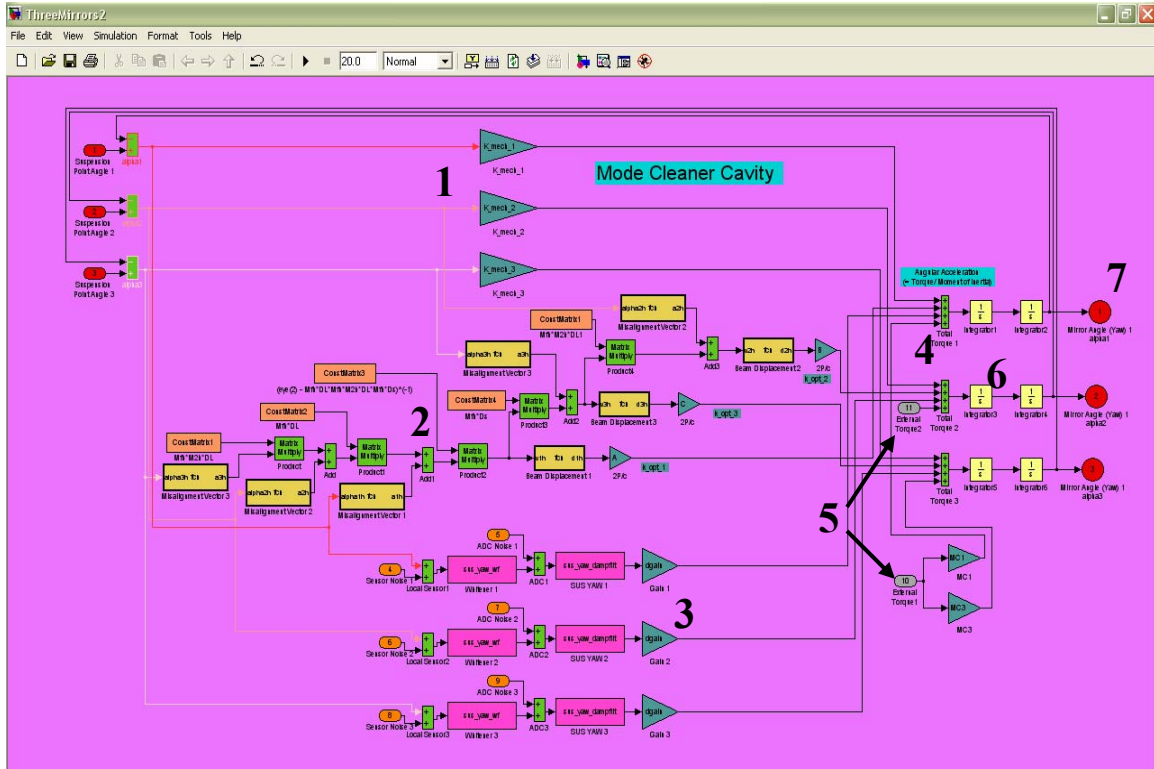


Figure 4: Screen shot of Simulink model of mode cleaner cavity, ThreeMirrors2.mdl.

The left side of the model (Figure 4) uses the current angular displacement positions of the three mirrors, and distributes that information to the three stiffness components: Stiffness due to the pendulum (1), stiffness due to radiation pressure (2), and stiffness due to the controls servo (3). These stiffness components are in units of angular acceleration, or torque per unit moment of inertia. The stiffness components are summed together (4) with optional external excitations (5). The signal is then integrated twice (6) to get to units of angle, and then the angles of each mirror are read back on the right side of the screen (7) to the left side of the screen to start again, as well as to an external plotting function. The pendulum and radiation pressure stiffness components are defined using the equations for τ_{pendulum} and $\tau_{\text{radiation}}$, and dividing by the moment of inertia of the mirrors, using the same formulae as the following analytic calculations. The radiation stiffness in particular utilizes matrix equations to determine beam position given the angles of the three mirrors, as derived by Sigg⁸, and described in the Analytic Calculations section below.

The script used to run the model (See Appendix A: Documentation of Simulink Model) outputs a bode plot of the transfer function, taken between the external excitation point (5 in Figure 4) and the desired mirror read-back (7 in Figure 4). The transfer function shows the peak resonant frequency of the mirror, given all the torques acting on it. As the power in the cavity is raised, thus increasing the torque due to radiation pressure, the peak is seen to move. The peaks moving to higher frequencies indicate that the self-aligning mode has been excited by the laser light, while peaks moving to lower frequencies indicate that the unstable mode has been excited.

In the case of the mode cleaner of the 40m interferometer at Caltech, when the curved MC2 mirror is excited in yaw and the angle of MC2 is examined (i.e. the transfer function is between the excitation of MC2, and the angle of MC2 itself), as the power is increased from 0W to 3W in 1W increments, the model predicts that the peak resonant frequency of the mirror shifts from 0.8241Hz with 0W incident on the mode cleaner to 0.8821Hz with 3W incident on the mode cleaner cavity (Figure 5).

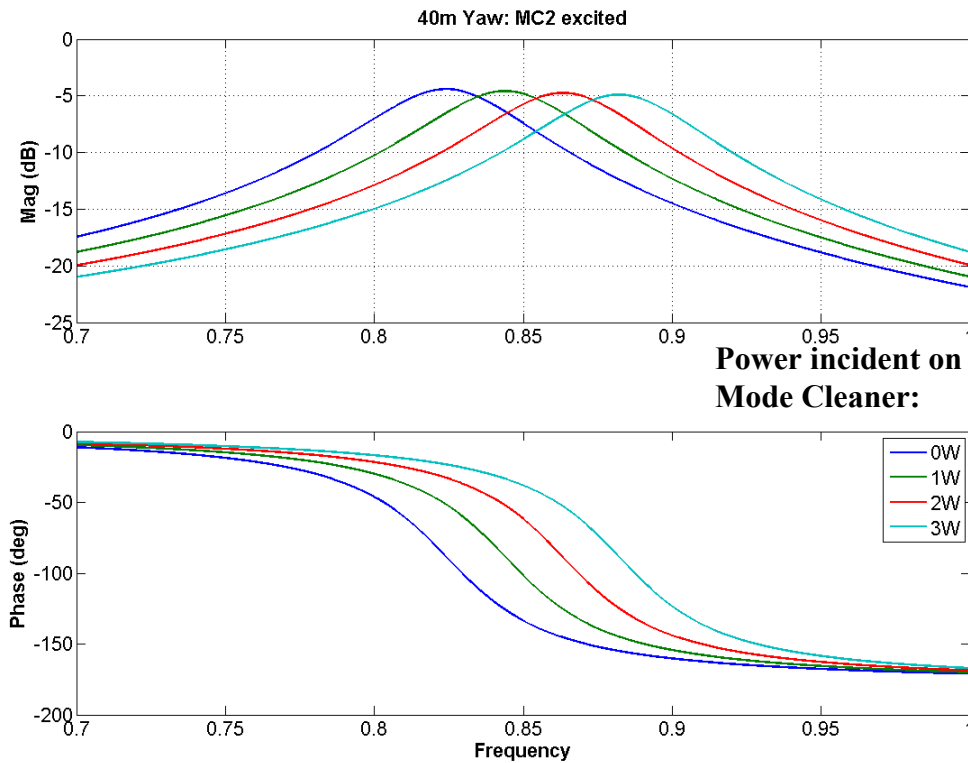


Figure 5: Example output of Simulink model. MC2 of the 40m interferometer has been excited in the yaw degree of freedom, with several different powers incident on the cavity.

For the case of the 40m interferometer's mode cleaner when MC2 is excited in pitch and the angle of the MC2 is examined, again as the power is increased between 0W and 3W, in 1W increments, the model predicts a much more complicated transfer function.

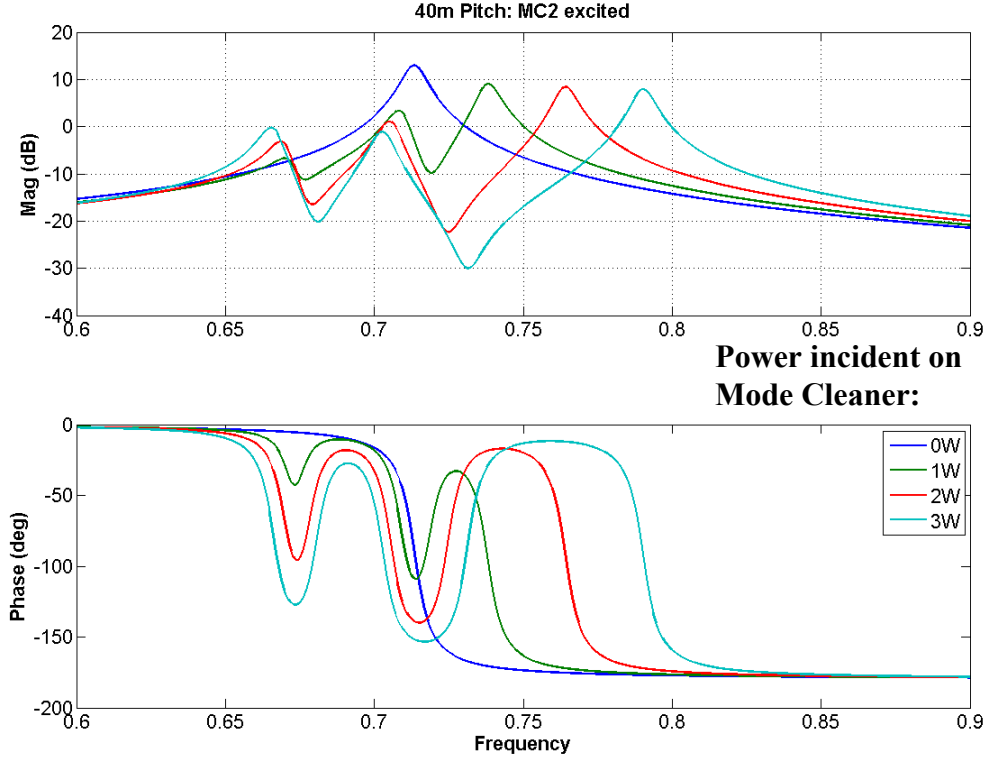


Figure 6: Example output of Simulink model. MC2 of the 40m interferometer has been excited in the pitch degree of freedom, with several different powers incident on the cavity.

Analytic Calculations

Before the model can be used to examine potential instabilities in LIGO interferometers, it must be checked for accuracy. These calculations were done to ensure that the model analytically matched literature. We briefly follow Sigg’s derivation of the “critical power” in a mode cleaner cavity, to compare the critical power calculated for the 40m interferometer’s mode cleaner to the modeled value.

Sigg has derived the following equations for describing the beam after leaving each mirror in a mode cleaner cavity:

$$\vec{v}_1 = \left(1 - M_f M_1 D_L M_f M_2 D_L M_f M_3 D_s\right)^{-1} \left(M_f M_1 D_L M_f M_2 D_L \vec{\alpha}_3 + M_f M_1 D_L \vec{\alpha}_2 + \vec{\alpha}_1\right)$$

$$\vec{v}_3 = M_f M_3 D_s \vec{v}_1 + \vec{\alpha}_3, \text{ and}$$

$$\vec{v}_2 = M_f M_2 D_L \vec{v}_3 + \vec{\alpha}_2,$$

where $\vec{v}_i = \begin{bmatrix} \text{position} \\ \text{slope} \end{bmatrix}$ of the beam after reflecting off the i^{th} mirror, and M_1, M_2, M_3 are

the ABCD matrices describing the beam’s reflection from MC1, MC2 and MC3 respectively. D_L and D_s are the ABCD matrices describing the free space propagation of the beam along lengths L and $2s$ as in Figure 3. M_f is the “flip matrix” defined as 1 for the pitch degree of freedom, and -1 for yaw, to account for the flipping of the coordinate system after reflecting off each mirror in the horizontal direction. $\vec{\alpha}_1, \vec{\alpha}_2, \vec{\alpha}_3$ are the

“misalignment vectors” that describe the angle of the mirror’s misalignment from the nominal axis⁸.

Sigg uses the beam position component from these equations, the long cavity limit, and takes into account the incident angle of the beam on the mirrors to arrive at the stiffness matrices for the horizontal and vertical cases for the mode cleaner cavity:

$$K(h) = \begin{bmatrix} 0 & 0 & 0 \\ 0 & -2 & 0 \\ 0 & 0 & -g \end{bmatrix}, \quad K(v) = \frac{1}{1-g} \begin{bmatrix} g & 0 & 1 \\ 0 & 0 & 0 \\ 1 & 0 & 1 \end{bmatrix}, \text{ where } g \text{ is the } g\text{-factor of the cavity,}$$

with $g = 1 - \frac{L}{R}$. For the mode cleaner cavities, R is taken to be the radius of curvature of

MC2⁸. The eigenvalues of these matrices are:

$$k(h)_1 = -2,$$

$$k(h)_2 = -1/g,$$

$$k(v)_1 = \frac{-1 - g + \sqrt{5 - 2g + g^2}}{2(g - 1)}, \text{ and}$$

$$k(v)_2 = \frac{-1 - g - \sqrt{5 - 2g + g^2}}{2(g - 1)}.$$

As in another of Sigg’s papers⁵, using the largest positive eigenvalue with the 40m interferometer’s mode cleaner parameters,

$$P_{crit} = \frac{Ic\omega_{pendulum}^2}{2kL} = \frac{(9.6068 * 10^{-5} \text{ kg} * m^2) (299792458 \text{ m/s}) (2\pi * 0.712 \text{ Hz})^2}{2(2.6609)(13.542 \text{ m})} = 7998.1 \text{ W}^5.$$

Here $I = \frac{1}{4}Mr^2 + \frac{1}{12}Mh^2$, where $I = 9.6068 * 10^{-5} \text{ kg} * m^2$ is the moment of inertia of the mirrors, $M = 0.238 \text{ kg}$ is the mass of the mirrors, $r = 0.0375 \text{ m}$ is the radius of the optics, $h = 0.025 \text{ m}$ is the thickness of the mirrors, c is the speed of light, $\omega_{pendulum} = 2\pi * 0.712 \text{ Hz}$ is the pendulum frequency for the degree of freedom associated with k , k is the largest positive eigenvalue from the stiffness matrices, with $L = 13.542 \text{ m}$ as the length of the mode cleaner cavity and the radius of curvature of MC2 = 21.21 m, so $g = 0.3615$.

This “critical power”, P_{crit} , defines the power circulating in the cavity when $\tau_{radiation} = \tau_{pendulum}$, with no controls servo present. $\tau_{radiation} = \tau_{pendulum}$ implies that the resonant peak of the mirrors is at 0Hz because the radiation torque exactly cancels the restoring force of the pendulum. As above, Sigg’s equations calculate that the critical power for the 40m interferometer’s mode cleaner is 10.26kW circulating (about 21W incident). The model predicts that the resonant peak of the mirrors will be at 0Hz when the power incident on the mode cleaner is about 38W. Multiplying by the buildup gain of the cavity 487 gets a prediction of 18.5kW circulating. This prediction is almost a factor of 2 higher than the calculated value. This difference should be reconcilable, since the model uses the same formulae as the theory to calculate the critical power, and since the model seems to match the experimental data (below) so closely.

It is interesting to note that the $k(v)$ ’s approach ∞ as the g -factor approaches 1 (i.e. an optically unstable cavity), which implies $P_{crit} \rightarrow 0$ as $g \rightarrow 1$. For the case of a two

mirror cavity which has a dependence on $\frac{1}{1 - g_1 g_2}$, where g_1 and g_2 are the g-factors of each mirror, the effect of radiation pressure becomes large as $|g_i| \rightarrow 1$.

Measuring the 40m Interferometer's Mode Cleaner

Another method used to check the model's accuracy was to compare a modeled prediction to actual measurements with the 40m interferometer's mode cleaner. As in Figure 5, the model predicts a slight peak shift in the yaw degree of freedom as the power incident on the cavity is increased, and as in Figure 6, the model predicts a more complex peaking structure for the pitch degree of freedom.

The response of the 40m lab's mode cleaner was measured using the swept sine function of Diagnostics Test Tools. Before taking measurements, the damping in the controls servos was reduced to allow the mirror's resonant peak to be clearly evident in the transfer functions. Based on the model's predictions, MC2 was chosen for these measurements, as it appeared to have the largest modeled peak shift. For the yaw measurement, MC2 was excited using the C1:IOO-MC2_YAW_EXC channel, and the Wave Front Sensor channels C1:IOO-WFS1_IY and C1:IOO-WFS2_IY were monitored. Transfer functions were taken between the excitation channel and the first Wave Front Sensor channel, and between the excitation channel and the second Wave Front Sensor channel. The coherence between the excitation and the WFS signals was also monitored. Since the WFS do not look at the angle of any one mirror directly, but rather see a combination of MC1, MC2 and MC3, it is possible that one, both, or neither WFS would see the result of exciting MC2. For the yaw case, WFS1 had good coherence throughout the measurement, while WFS2 lost coherence regularly, so only the result from WFS1 is shown below. Figure 7 shows the results of this yaw measurement, taken with several different laser powers incident on the mode cleaner cavity. 0.322W represents a fairly low power, 0.974W represents an average power during normal operation at the 40m, and 1.953W was the maximum amount of power we were able to get to the mode cleaner for practical reasons. For each power level, the measurement was taken, and immediately afterward the power into the mode cleaner was measured with a Scientech Vector S310 Power Meter. As a result of the different power levels circulating in the cavity, the measured magnitude of the transfer functions was different for each measurement, so they have been normalized such that they all have the same magnitude at 1.2Hz. As was predicted by the model, the resonant peak for the yaw degree of freedom moved to higher frequencies as the power in the cavity increased.

For the pitch case, analogous channels were excited and monitored, and the same powers were incident on the mode cleaner cavity. Both WFS1 and WFS2 had good coherence throughout the measurement, so six transfer functions are plotted in Figure 8, two for each power. While the peak shift is visible for the 1.953W measurement, there is no discernable peak shift between the two lower powers. This is likely because the pitch degree of freedom is much more strongly coupled to the pos, or position, degree than yaw is. As the pos degree of freedom must be controlled to keep the cavity in lock during the measurement, the pitch measurement is not in fact just pitch. This coupling between the pitch and pos degrees of freedom is not incorporated into the Simulink model. We do however see an expected peak split for the 1.953W measurement, similar to that predicted in the model.

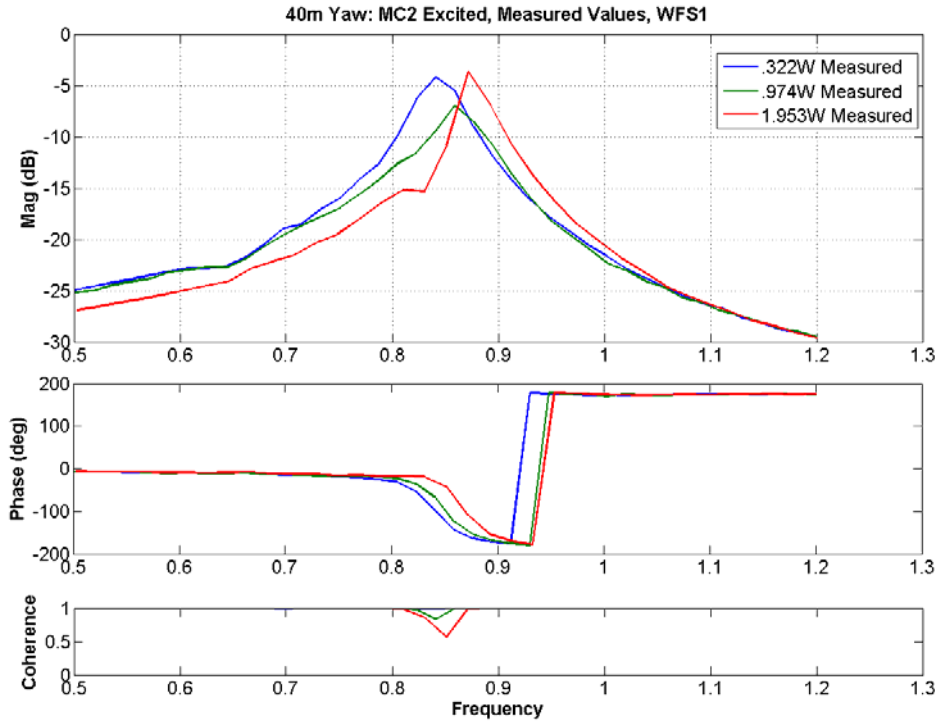


Figure 7: Measured transfer functions between MC2 and WFS1, for the yaw degree of freedom, with several different powers incident on the mode cleaner cavity.

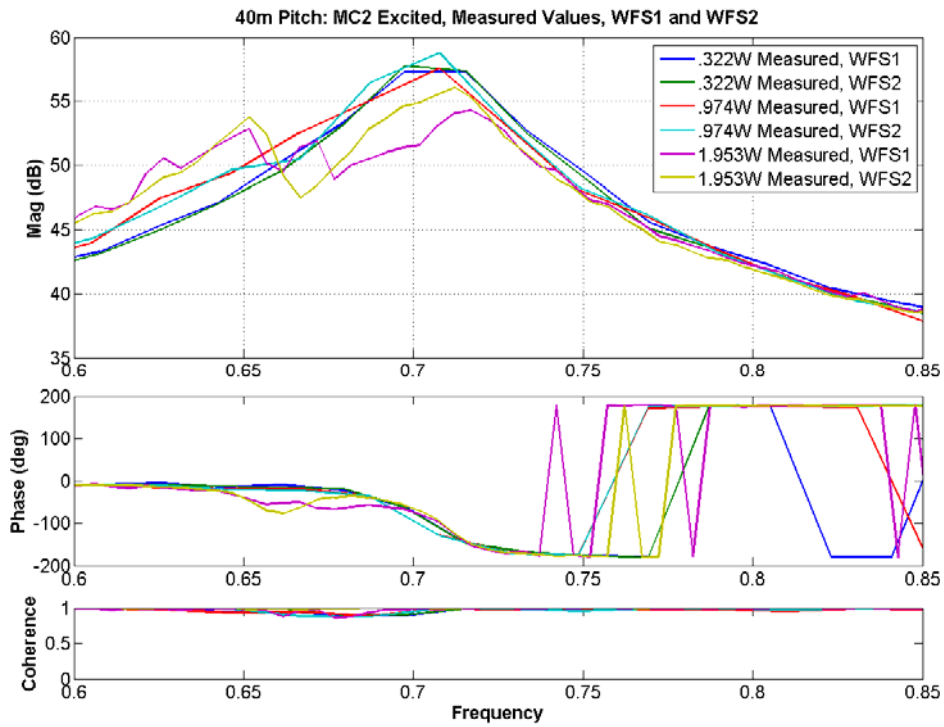


Figure 8: Measured transfer functions between MC2 and WFS1 and MC2 and WFS2, for the pitch degree of freedom, with several different powers incident on the mode cleaner cavity.

Figure 9 superimposes the peaks from Figure 5 and Figure 7 to show the consistency between the modeled and the measured transfer functions of the 40m interferometer’s mode cleaner, particularly in the yaw degree of freedom. For this plot of the modeled values, the pendulum frequency was taken to be 0.824Hz instead of the measured 0.814Hz, to give a best fit to the lowest measured peak frequency. This 0.01Hz discrepancy may be due to the value for the measured pendulum frequency having been measured while the mirrors were hanging freely, while the measurements here were made while the mode cleaner was in lock.

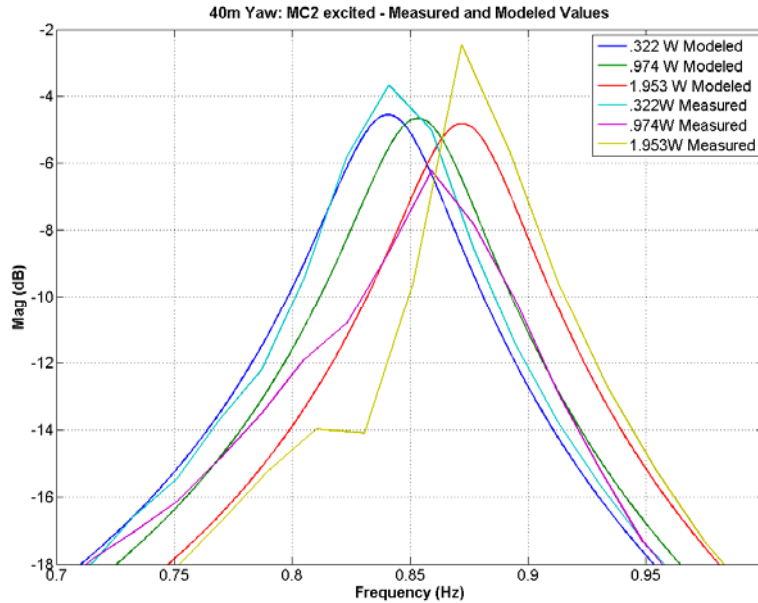


Figure 9: Measured and modeled transfer functions of the yaw degree of freedom superimposed on the same plot.

Conclusions from Measurements and the Model

Since we now have a model of the LIGO mode cleaner cavities that is consistent with calculations and measurements of the 40m interferometer’s mode cleaner, we can extrapolate the model and use it to examine the mode cleaners in the upgrades of LIGO. Toward this end, I studied the relative changes in the modeled resonant peak frequencies between Initial LIGO and Enhanced LIGO, and between Initial LIGO and Advanced LIGO. The larger the effect of the radiation pressure, the more the peak will shift, and so the more concerned we should be about potential instabilities in the future mode cleaners. Looking at the change in peak shifts from Initial LIGO to the upgrades gives a baseline existing, measurable cavity that is known to be stable, to compare the upgrades to. It seems that if the ratio of the peak shifts between Initial LIGO and an upgrade is 1, they will be equally stable, if the ratio is smaller than 1, the upgrade will be more stable, and if the ratio is greater than 1, the upgrade will not be as stable as Initial LIGO, although how much more unstable is a further question.

Table 1 shows the resonant peak frequencies for the three versions of LIGO, for the case of no power in the cavity, and the maximum possible laser power incident on the cavity. The final column is the difference between maximum power and no power incident on the cavity. For the pitch case, the resonant peak splits, so the sub-columns

indicate the change from the original peak to the new, lower peak, and from the original peak to the upper peak.

	0W	Maximum Power (10W, 30W or 200W)		Change in Peak Frequency	
Initial LIGO YAW	0.8834Hz	1.1016Hz		0.2182Hz	
Enhanced LIGO YAW	0.8834Hz	1.239Hz		0.3556Hz	
Advanced LIGO YAW	1.095Hz	1.162Hz		0.0670Hz	
Initial LIGO PITCH	0.8123Hz	Lower Peak 0.7503Hz	Upper Peak 1.048Hz	Lower Peak -0.062Hz	Upper Peak 0.2357Hz
Enhanced LIGO PITCH	0.8123Hz	0.6211Hz	1.398Hz	-0.1912Hz	0.5857Hz
Advanced LIGO PITCH	1.095Hz	1.072Hz	1.159Hz	-0.023Hz	0.0640Hz

Table 1: Resonant peak frequencies at different power levels in LIGO upgrades, and the change in peak frequencies.

Table 2 shows the ratios of amount of peak frequency change, between Initial LIGO and the LIGO upgrades, for pitch and yaw.

	YAW	PITCH, Lower Peak	PITCH, Upper Peak
Enhanced LIGO Initial LIGO	1.63	3.08	2.48
Advanced LIGO Initial LIGO	0.31	0.37	0.27

Table 2: Ratios of amount of change in peak frequencies.

The increase in the size of the peak shift between Initial LIGO and Enhanced LIGO seems obvious as the cavity parameters will not change during the upgrade, so the pendulum torque will remain constant, but the torque due to radiation pressure will go up by a factor of 3, with the increase in laser power from 10W to 30W. The decrease in the amount of peak shift between Initial LIGO and Advanced LIGO despite the factor of 20 increase in laser power is explained by the factor of approximately 60 increase in the pendulum torque. The mass of the mode cleaner mirrors will be increased from 0.243kg to 3.04kg, the radius of the mirrors will be doubled from 0.0375m to 0.075m, and the thickness of the mirrors will be increased from 0.025m to 0.08m. This translates to a change from $9.8086 \cdot 10^{-5} \text{ kg} \cdot \text{m}^2$ to $0.0059 \text{ kg} \cdot \text{m}^2$ in the moment of inertia of the mirrors. Since the pendulum torque is directly proportional to the moment of inertia of the mirrors, this implies that the pendulum torque will increase by a factor of 60.15 due to the change in moment of inertia between Initial LIGO and Advanced LIGO.

Showing the same table again (Table 3), with the ratios of the pendulum and radiation torques makes it clear that the shift in resonant peak frequencies is dependent on this ratio. If the change in pendulum frequency is left out of the ratios in the 4th column of Table 3 and only the change in moment of inertia is considered for the pendulum

torque's change, the ratio for the Advanced LIGO case approaches 0.33 rather than the quoted 0.22.

	YAW	PITCH Lower Peak	PITCH Upper Peak	$\frac{\tau_{\text{radiation}}}{\tau_{\text{pendulum}}}$
<u>Enhanced LIGO</u> <u>Initial LIGO</u>	1.63	3.08	2.48	3
<u>Advanced LIGO</u> <u>Initial LIGO</u>	0.31	0.37	0.27	0.22

Table 3: Ratios of amount of change in peak frequencies and ratio of change in contributing torques.

As the sensitivity for Enhanced LIGO will be similar to that of Initial LIGO, the slight increase in peak movement should be within the range of the current Wave Front Sensors controls servo, without concern that the servo will limit LIGO's sensitivity. For Advanced LIGO, this model needs to be reconfirmed after triple pendulum systems have been added to the model, but with the assumption of single suspension systems, the Advanced LIGO Mode cleaners are predicted to be more stable than the Initial LIGO mode cleaners. This implies that the current design parameters for the Advanced LIGO mode cleaners may have plenty of flexibility before radiation pressure is a significant concern. Thus decisions can be made with other considerations weighed more heavily. For example, the radius of curvature of MC2 could be increased, which would bring the g-factor of the cavity closer to 1, but would also increase the beam size on MC1 and MC3, allowing the beam to average out more of the Brownian noise of the mirror's coatings. Again, this information must be reexamined using a version of this model that incorporates the quad pendulum systems, rather than using the assumption of single suspension systems.

Improving the Mode Cleaner Servo

Prior to taking measurements to check the model, the then-current mode cleaner servo was checked to ensure that it was working properly. It had previously been noticed that there was an overly large amount of noise at 3.710MHz, the beat frequency between two of the sideband frequencies that are added to the main carrier light to control the interferometer. Since the mode cleaner servo circuit board includes op-amps, a signal at such a high frequency is undesirable, because it can cause the op-amps to run into their slew rates. To alleviate this problem, a low-pass Butterworth Pi filter with a notch was built. The low-pass filter has a pole at 1MHz, and the notch is tuned to be at 3.710MHz. Figure 10 and Figure 11 show the circuit diagram of the filter, and a photo of the finished filter.

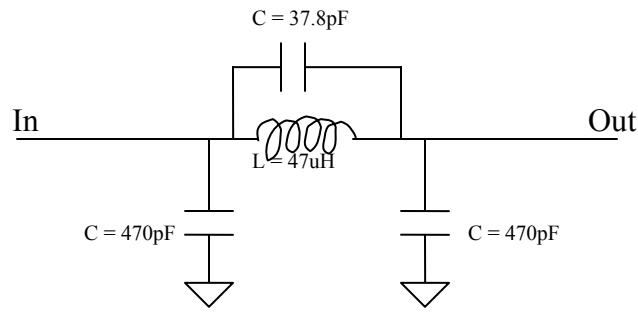


Figure 10: Circuit diagram of Butterworth Pi low-pass filter with a notch, for mode cleaner Servo.

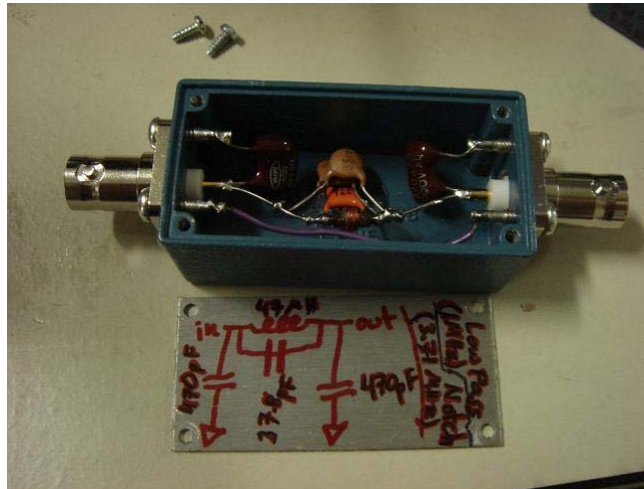


Figure 11: Photo of Butterworth Pi low-pass filter with a notch, for mode cleaner Servo.

While initially measuring the mode cleaner servo to understand what its gain looked like before inserting the filter, it was unclear what the servo's circuit board was doing. Upon inspection, it was noticed that modifications had been made to the board that had not been noted on the schematic of what the board should look like. This helped initiate the installation of the new mode cleaner servo board. It is hoped that installing the new circuit board and resolving the problem of the 3.710MHz signal will improve the mode cleaner servo, and help control the entire interferometer more efficiently.

Amplitude Modulated Laser to Check Radio Frequency Photodiodes

Another important check done to ensure the measurements of the 40m interferometer's mode cleaner were as accurate as possible was to verify that the photodiodes in the system were working as expected. To do this, an amplitude modulated (AM) laser (Figure 12) was assembled to test all of the radio frequency (RF) photodiodes at the 40m interferometer, including those in the mode cleaner servo. The various RF photodiodes are tuned to be sensitive to particular frequencies of light corresponding to the beats between the carrier and the RF sidebands, or between the different sidebands that are added to the main laser light to assist with controlling the interferometer. Using the AM laser to do swept sine measurements of all the photodiodes is useful, to ensure that they are tuned to the correct frequencies. The laser emits light at 1064nm, the same wavelength as the main laser used in the interferometer, so the

photodiodes should respond to the AM laser just as they would to the main laser. The AM laser's transfer function was taken using a New Focus 1611 photodiode, and is fairly flat out to 500MHz, well above the highest frequency the RF photodiodes are tuned to (See Appendix B: AM Laser Documentation and Parts List for full beam profile data). The laser is powered by a Lightwave Precision Current Source for DC, and can have RF modulations added through the bias tee in the upper right corner of Figure 12. The laser diode is housed inside a small box (labeled "Laser" in Figure 12), and is fiber-coupled. The fiber travels through the blue tubing shown in the figure, which will hold its shape, making it convenient to shine light into all the photodiodes. The fiber then sends the light through a lens mounted on the end of the tube.



Figure 12: AM Laser. The laser diode is in the box labeled "Laser", and is fiber-coupled. The fiber travels through the blue tubing, and sends the light through a lens at the end of the tube.

The laser was used to do swept sine measurements of almost all of the RF photodiodes used with the 40m interferometer. An HP4395A Network Analyzer was used to provide the RF modulation to the laser, and to take the transfer function between the laser's modulation, and the "RF Out" of the photodiodes. While taking measurements, the DC voltage of the photodiodes was monitored, to ensure that the maximum amount of laser light possible was hitting the photodiode. See Appendix C: RF Photodiode Data for transfer functions of all the RF photodiodes in the 40m lab. As an example, the transfer function of the photodiode monitoring the reflected light from the Mode cleaner known as "MC REFL" is shown in Figure 13. This photodiode signal is amplified by a tank circuit designed to peak at 29MHz, which is what is observed in Figure 13. The schematic of the photodiode is LIGO document number D980454-03-C⁹.

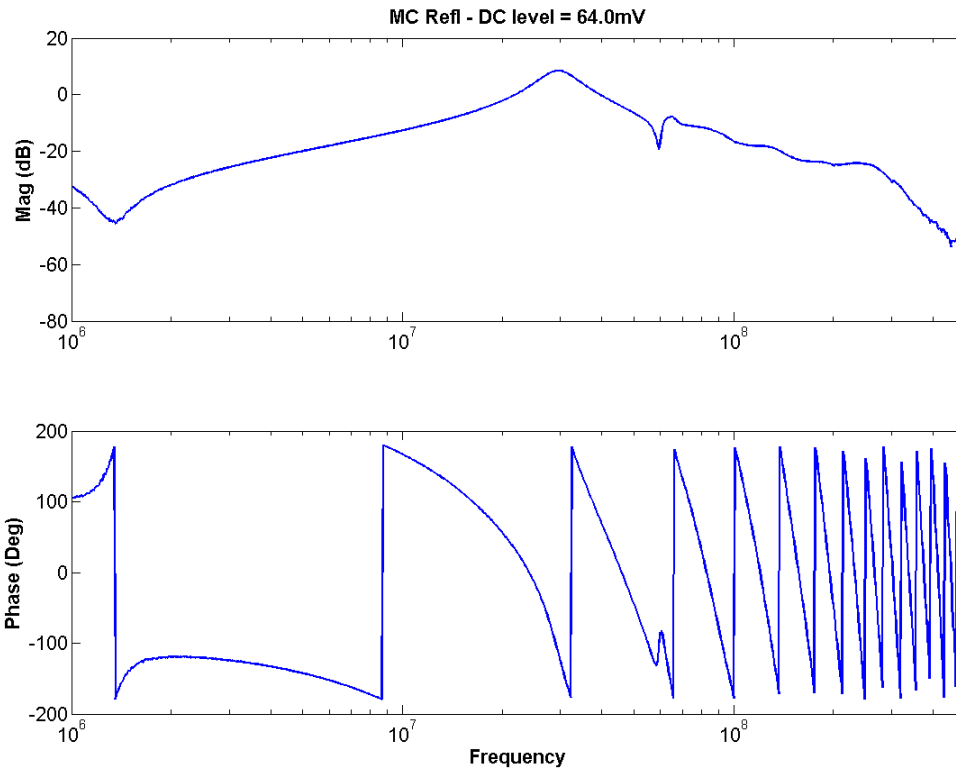


Figure 13: Transfer function taken by AM laser of MC Refl, the RF photodiode monitoring the light reflected off the mode cleaner cavity.

This summer a model has been written that depicts the 40m interferometer's mode cleaner. The model matches experimental data, and is consistent with the theory to closer than a factor of 2. Since the model and the theory use the same formulae to calculate the critical power in a cavity, further examination should resolve this discrepancy. Overall, the model does a reasonable job of modeling the 40m interferometer's mode cleaner, and so this model can later be incorporated into a larger model that includes triple-pendulum systems, and can then be used to accurately model the Advanced LIGO mode cleaners. In addition, an AM laser has been assembled in order to test RF photodiodes, and a filter has been prepared to improve the mode cleaner servo.

I would like to thank Alan Weinstein and Rana Adhikari for being my mentors this summer, and for their excellent guidance. Thank you to Sam Waldman, other Summer 2006 SURF students, the rest of the 40m lab at Caltech for helping along the way, and LIGO Engineering. Thanks also to the LIGO NSF REU Program and the Caltech SURF Program for making this project possible.

Appendix A: Documentation of Simulink Model

The following MATLAB script is used to run the Simulink model, and plot the predicted transfer function between the external excitation point, and the mirror's angle.

```

%M-File to run ThreeMirrors2.mdl

%This version models the YAW Degree of Freedom for the 40m
%interferometer's mode cleaner cavity

%This script returns a state-space object "sys" which represents the
%model, and plots a transfer function between an excitation and a
%mirror readout point.

f = logspace(-1,1,1000);

%-----Mode of Driving, when exciting MC1 and / or MC3-----

MC1 = 1;
MC3 = -1;

%-----Variables-----

Pinc = 0;           %Power incident on the mode cleaner, in Watts
P = Pinc*487;      %Power circulating in the MC, in Watts
c = 299792458;     %Speed of Light, in m/s

w1 = 2*pi*.836;    %Measured yaw pendulum frequency, in Hz
M1 = .238;         %Mass of mirror, in kg
h1 = .025;        %Thickness of mirror, in m
R1 = 1000000000;   %Radius of CURVATURE of optic, in m
r1 = .075/2;      %Radius of optic, in m

w3 = 2*pi*.814;    %Measured yaw pendulum frequency, in Hz
M3 = .238;         %Mass of mirror, in kg
h3 = .025;        %Thickness of mirror, in m
R3 = 1000000000;   %Radius of CURVATURE of optic, in m
r3 = .075/2;      %Radius of optic, in m

w2 = 2*pi*.814;    %Measured yaw pendulum frequency, in Hz
M2 = .238;         %Mass of mirror, in kg
h2 = .025;        %Thickness of mirror, in m
R2 = 21.21;       %Radius of CURVATURE of optic, in m
r2 = .075/2;      %Radius of optic, in m

Lmc = 13.542;      %Length of Mode cleaner Cavity, in m
%-----Finding Beam Positions-----
%These equations as defined in Sigg's T030275.

%Mf = flip matrix to account for the change in coordinates after
%reflecting off a mirror
Mfh = [...
    -1 0
    0 -1];

%M2 = ABCD matrix for reflecting off the curved mirror
M2h = [...
    1 0
    -2/R2 1];

```

```

%Matrix for the free space propagation along one of the long sides of
the
%triangle
DL = [...
    1 Lmc
    0 1];

%Matrix for free space propagation along the short side of the triangle
Ds = [...
    1 0
    0 1];

%Matrix equations to define the position of the beam after reflecting
%off each mirror:
ConstMatrix1 = Mfh*M2h*DL;
ConstMatrix2 = Mfh*DL;
ConstMatrix3 = (eye(2) - Mfh*DL*Mfh*M2h*DL*Mfh*Dc)^(-1);
ConstMatrix4 = Mfh*Dc;

%-----Calculate k's-----
%Mechanical (pendulum) K's:
K_mech_1 = w1^2;
K_mech_3 = w2^2;
K_mech_2 = w2^2;

%Optical (radiation pressure) K's (Divide by Moment of Inertia to get
%into units of Angular Acceleration):

Inertia1 = 1/4*M1*r1^2+1/12*M1*h1^2;
Inertia2 = 1/4*M2*r2^2+1/12*M2*h2^2;
Inertia3 = 1/4*M3*r3^2+1/12*M3*h3^2;
%Negative signs to take into account the beam's flipping when going
%around in yaw:
A = -2*P/c*Inertia1;
B = -2*P/c*Inertia2;
C = -2*P/c*Inertia3;

%YAW mode damping gain
dgain = 6.5;
sus_wf = zpk(-2*pi*3, -2*pi*[30,100], 2*pi*30*100/3);
%onlinefilter function imports the digital filters.
lowpass = onlinefilter('C1SUS_MC2.txt', 'SUSYAW', 0, 1, 3, 4, 'analogSYS');
sus_dampfilt = lowpass;
% -----Run the Simulation!-----
[a,b,c,d] = linmod('ThreeMirrors2');
sys = ss(a,b,c,d);

%sys(2,11) excites input 11, and reads the value at output 2
Stability = mybodesys(sys(2,11),f);
% -----Plot it-----
mybodeplot(f,Stability)
grid
xlabel('Frequency [Hz]')
axis tight

```

Appendix B: AM Laser Documentation and Parts List

- GTRAN GaAs Strained QW Laser Diode, Part # LD-1060.
- ILX Lightwave Precision Current Source, Part # LDX-3412.
- Mini-Circuits Coaxial Bias Tee, Part # ZFBT-4R2GW-FT.
- Pomona Electronics box, Part # 3231 (one BNC connector removed, hole drilled larger to fit laser's FC fiber connector through).
- LOCKWOOD PRODUCTS, INC. www.loc-line.com:
 - 2 51801 2-Segments, 5½" Long, ½" System
 - 1 51805 ½" NPT Connectors – Pack of 4
 - 1 78002 One ½" Hose Assembly Pliers
- Thorlabs:
 - 1 SM1CP2M End Cap for Machining, External Threads, SM1 Series
 - 1 SM1FC SM1 to FC Adapter
 - 1 SM1L10 SM1 Lens Tube 1" Deep
 - 1 S1TM08 SM1 Mounting Adapter Compatible with M8-.5 Threaded Lens Cells
 - 1 C440TM-C Mounted Lens, AR Coated 1050-1600nm
 - Notes: ½" NPT Tap drilled in End Cap, to attach lens assembly to Loc-Line Tubing.
 - Lens mounted in Lens tube, all the way at the front of the tube.
 - Fiber mounted as close to lens as possible.
- 9-pin D-sub connector socket .
- Sheet metal (1.5 inches x 3 inches), bent into "L" shape, one side hole punched to house 9-pin D-sub connector socket.
- 2 pins from an IC Socket (cut the plastic socket and remove just two bare pins) used to connect Pomona box BNC to laser diode.
- Brass (or other) plate for mounting onto (4 inches x 8 inches).
- 4 rubber feet for bottom of brass plate.
- 2 capacitors (100microF polarized electrolytic and 100nanoF ceramic) to clean up DC signal into bias tee.
- Custom length SMA cable just long enough to connect bias tee to Pomona box.
- Barrel-through adapters to connect bias tee to Pomona box.
- Rubber grommet to protect fiber from edge of hole in Pomona box.
- 2 strain relief clamps to hold Loc-Line Tubing to brass plate.
- Foam to protect coiled length of fiber between Pomona box and tubing.
- Sheet metal to cover foam, protect coiled length of fiber. Sharp edges wrapped in copper tape.
- Thermalcote Thermal Joint Compound – applied between Pomona box and brass plate, and laser diode and Pomona box.
- 5 minute epoxy to secure laser diode to Pomona box.
 - Notes: Transfer function of laser depended on position of laser in Pomona box. Best result when laser diode adhered as close to BNC connector as possible.

Pinout:

Lightwave Current Source:

Pin 1 connected to Pin 2

Pin 4 connected to Pin 5

Pin 8 connected to Pin 9

Pin 9 to GND of Bias Tee
Pin 5 to DC of Bias Tee

Laser Diode:

Pin 5 to GND of Pomona Box BNC (GND of RF+DC of bias tee)
Pin 9 to Center of Pomona Box BNC (Center pin of RF+DC of bias tee)

Focus point \cong .375 inches from end of lens tube
1mW of power when given 20.0mA current, DC

Figure 14 shows the AM laser's beam profile at the focus point:

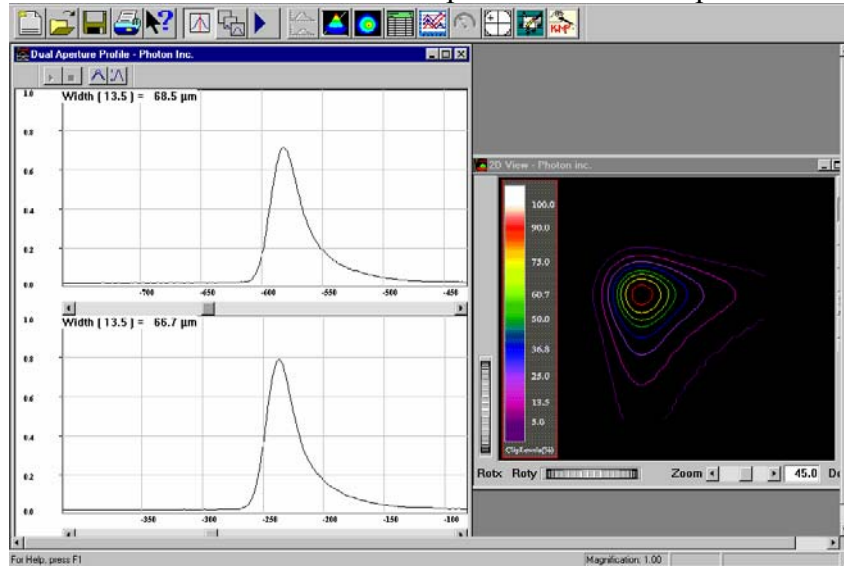


Figure 14: AM laser's beam profile, using beam scan.

Figure 15 shows the AM laser's transfer function, taken with New Focus 1611 Photodiode. Scale is from 10Hz to 500MHz, log scale. The noisy portion below 100kHz is due to the Bias Tee which is rated for 100kHz and higher.

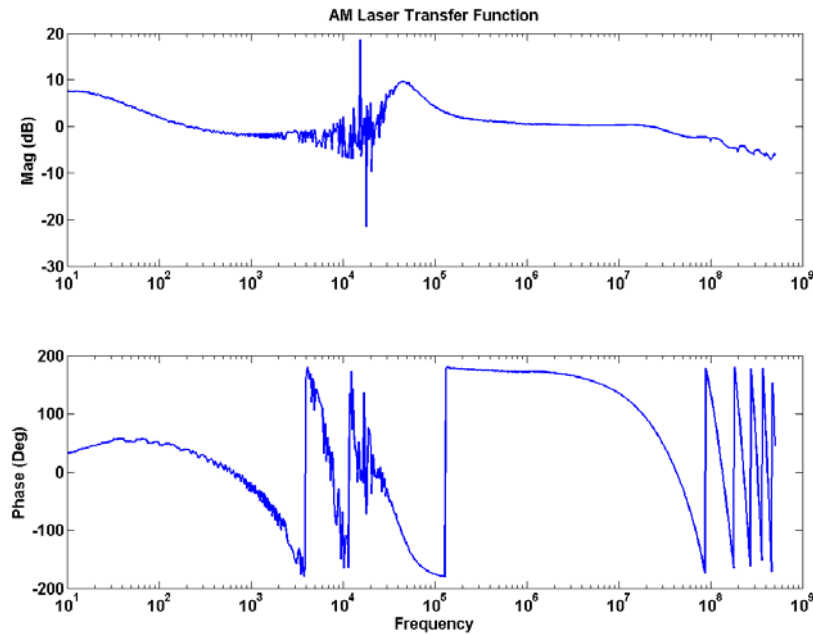


Figure 15: Transfer function of AM laser.

Figure 16 and Figure 17 show photos of the AM laser, without and with covers:

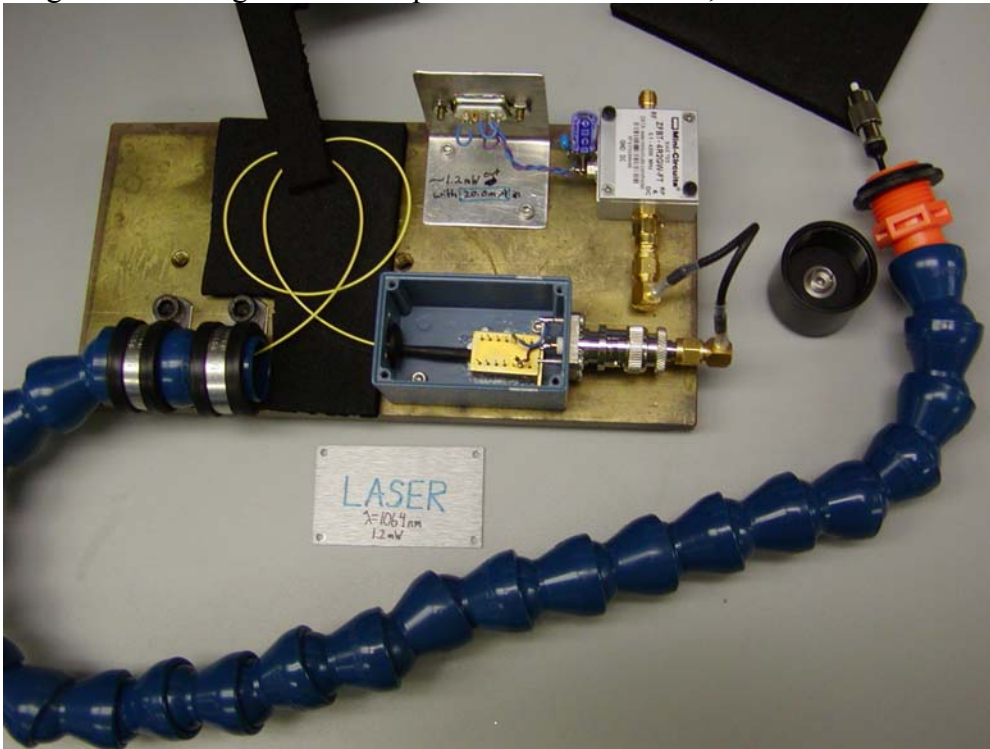


Figure 16: AM laser, partially disassembled. The fiber's FC connector exits the orange end of the tube, and screws into the lens tube. The laser diode is connected to the BNC on the side of the blue box via bare pins from an IC socket.



Figure 17: AM laser, fully assembled. A layer of foam and sheet metal has been added to protect the coiled section of fiber.

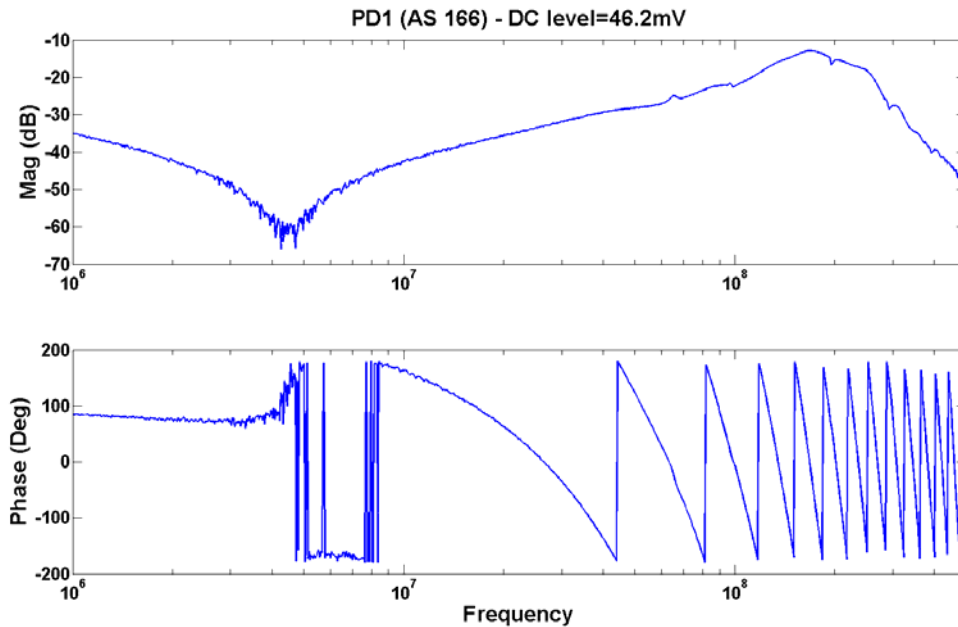
Appendix C: RF Photodiode Data

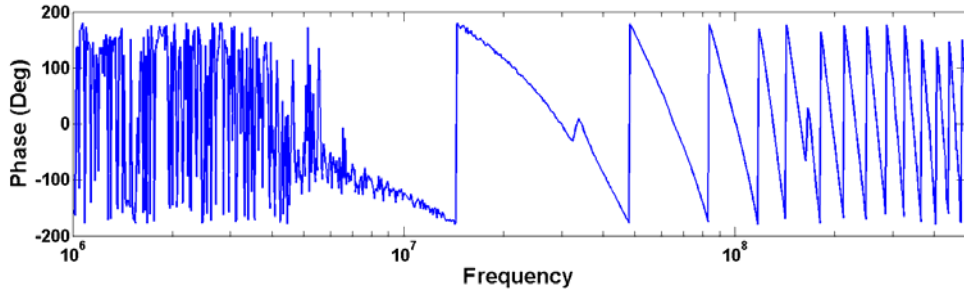
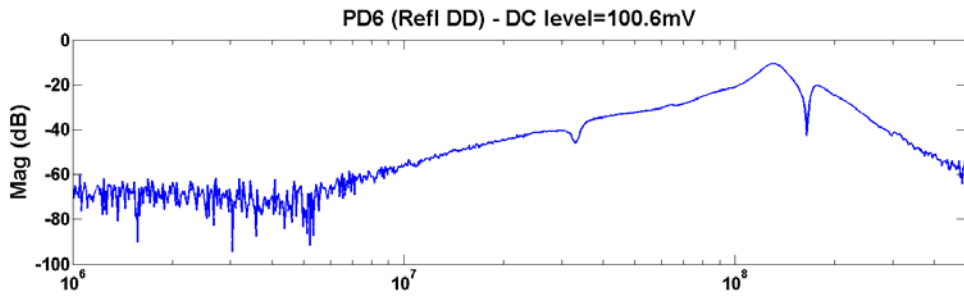
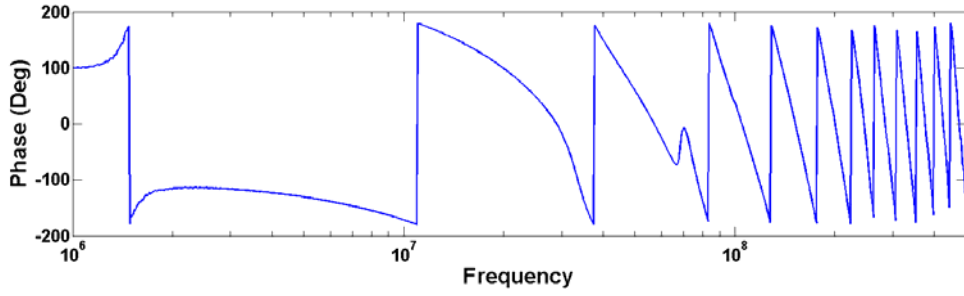
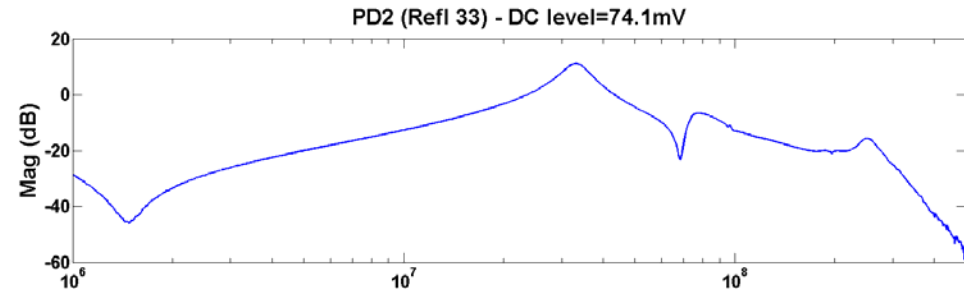
The following measurements were taken using an HP4395A network analyzer, with a power level of -10dBm. Each measurement has 801 points. The plots are transfer functions between the RF source to the AM laser and the response of the “RF Out” of the RF photodiode being measured. The AM laser’s constant current source was set to output 20.0mA. The DC Out of each photodiode was monitored using a digital voltmeter, and the value recorded in the title of each plot.

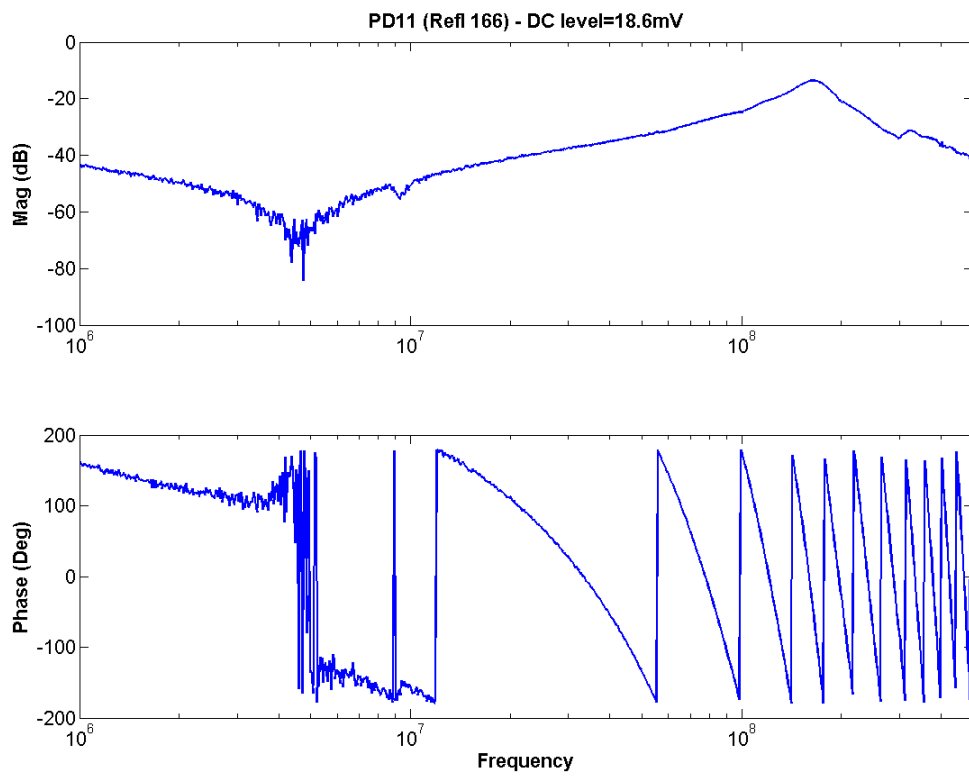
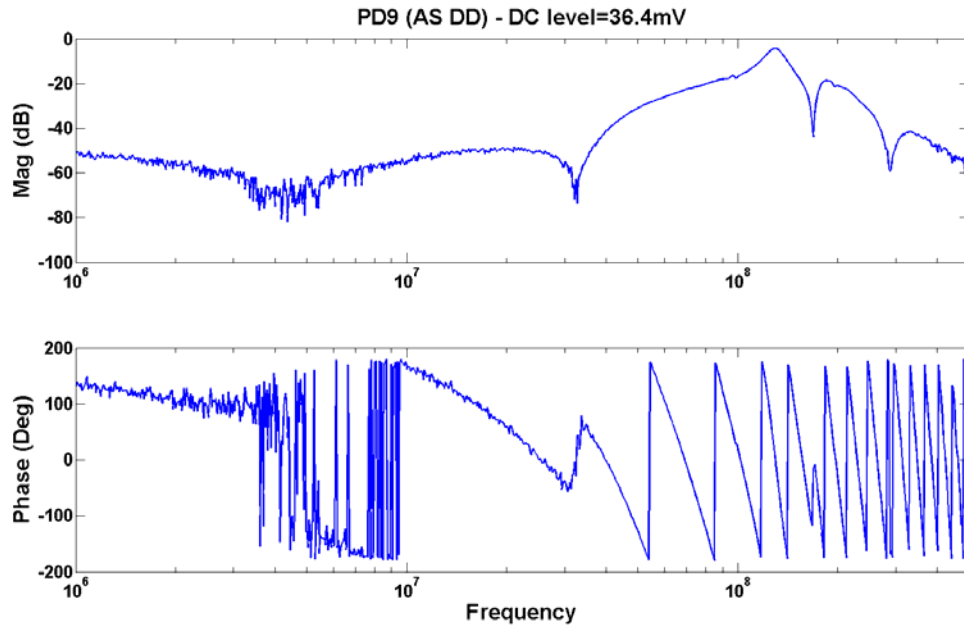
Photodiode, location, DC level (mV), notches, peaks

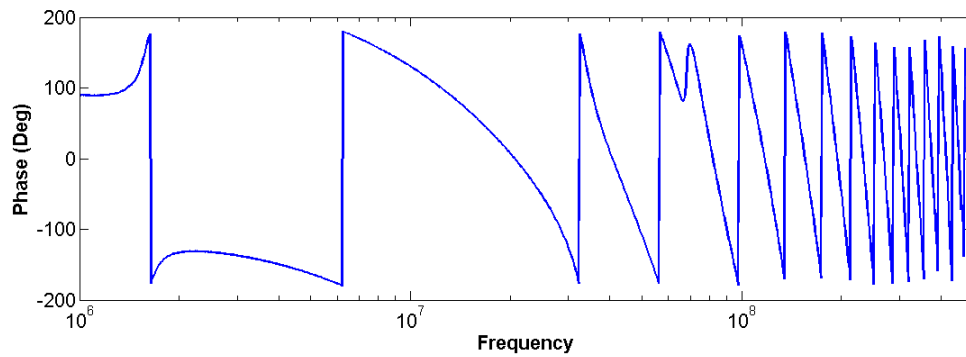
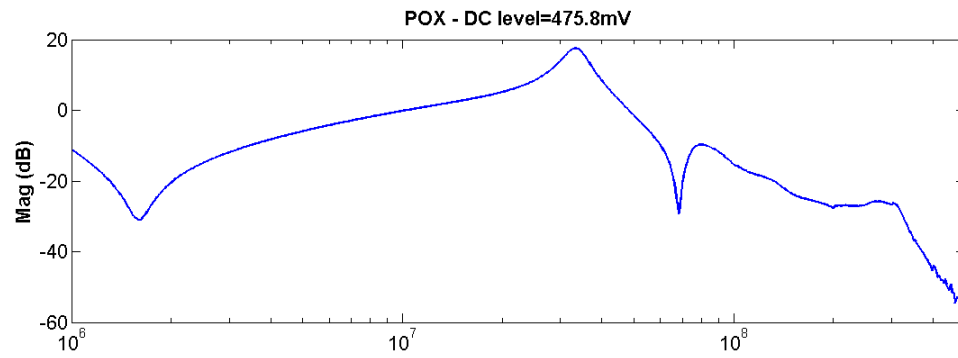
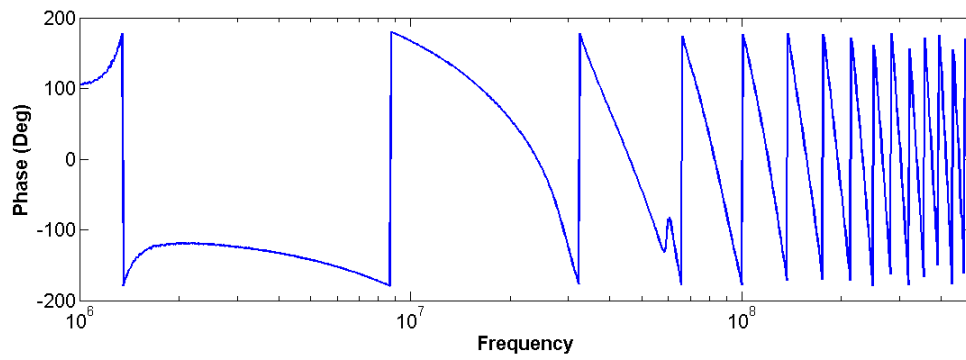
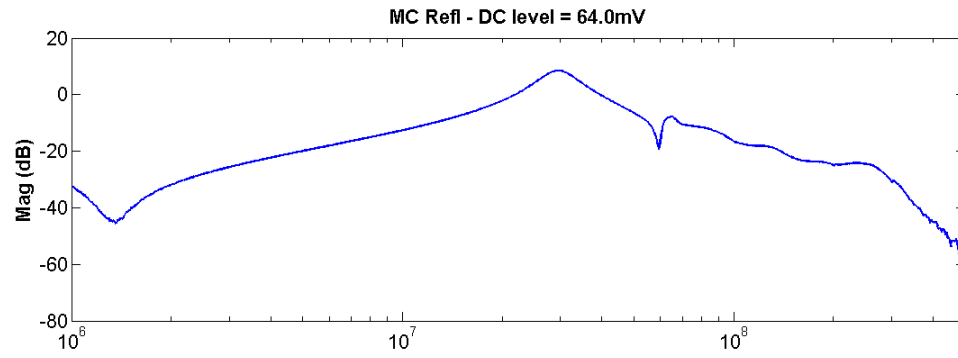
Photodiode	Location	DC Level	Notches (MHz)	Peaks (MHz)
PD 1 (AS 166)	AS Table	46.2 mV		168
PD 2 (Refl 33)	AS Table	74.1 mV	68	33, 251
PD 6 (Refl DD)	AS Table	100.6 mV	165	130
PD 9 (AS DD)	AS Table	36.4 mV	33, 169, 288	130
PD 11 (Refl 166)	AS Table	18.6 mV		165
MC Refl	AS Table	64.0 mV	60	29
POX	ITMX Table	475.8 mV	68	33
POY	ITMX Table	627.5 mV	68	33
POB	ITMY Table	231.2 mV	33, 166	131
SPOB	ITMY Table	892 mV		55, 253
MZ 29.485	PSL Table	60.9 mV	61	30

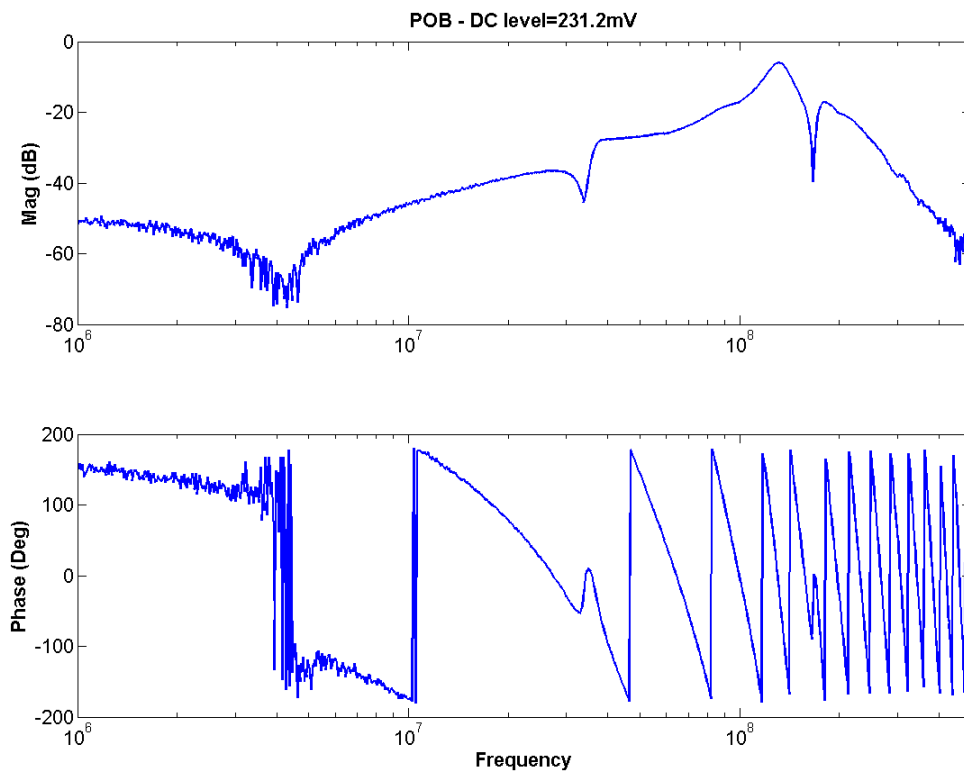
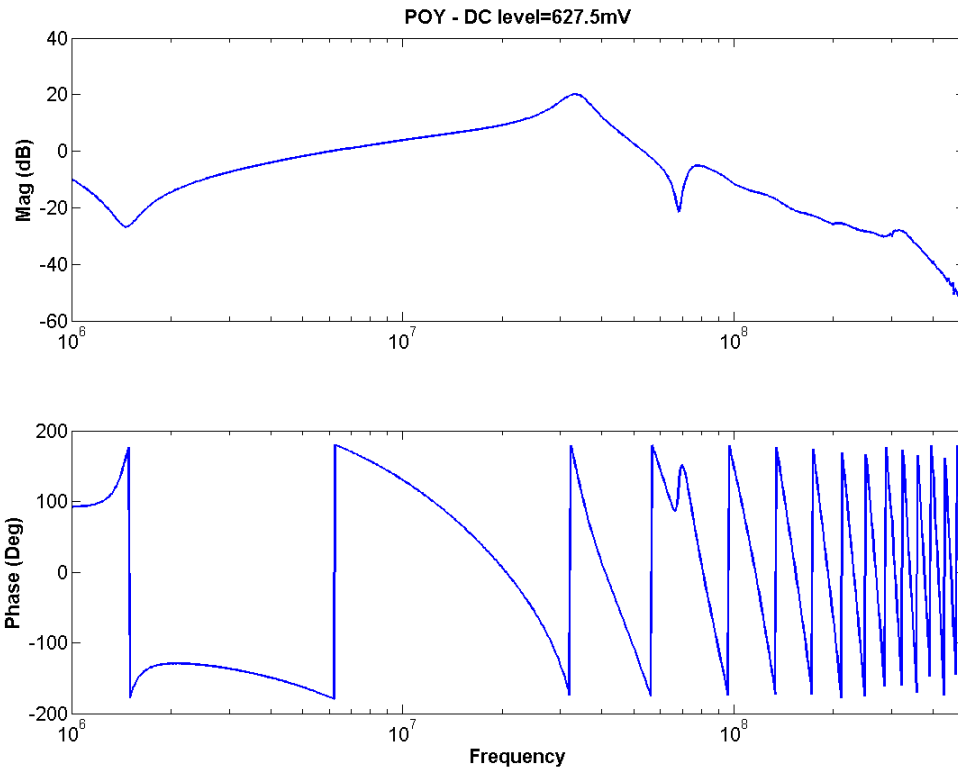
Table 4: Summary of RF Photodiode Data

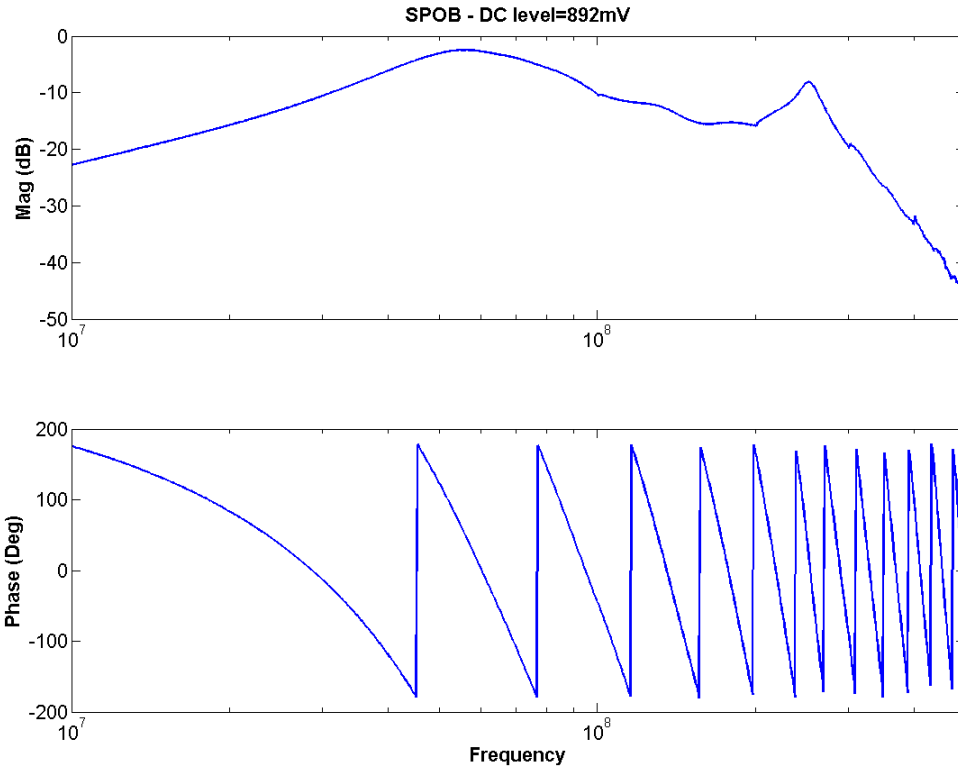












¹Misner, C.W., K.S. Thorne and J.A. Wheeler. *Gravitation*. W.H. Freeman and Co.: San Francisco. 1973.

²Weinstein, Alan. SURF Lectures. June 2006.

³Ward, Robert. "The Caltech 40m Prototype Detuned RSE Interferometer". NAOJ Seminar. 1 Mar 2006.

⁴Weinstein, Alan. Personal Interview. 25 Apr 2006.

⁵Sigg, Daniel. "Angular Instabilities in High Power Fabry-Perot Cavities". LIGO-T030120-00. 15 June 2003.

⁶Sidles, John A., Sigg, Daniel. "Optical Torques in Suspended Fabry-Perot Interferometers". LIGO-P030055-C. 26 January 2006.

⁷Adhikari, Rana. Personal Interview. 12 August 2006.

⁸Sigg, Daniel. "Angular Stability in a Triangular Fabry-Perot Cavity". LIGO-T030275-00. 2 December 2003.

⁹Suina, J., Ouimette, D. "LSC Photodiode". D980454-03-C. 7 January 2000.